JOURNAL OF THERMOPHYSICS AND HEAT TRANSFER
Vol. 22, No. 3, July–September 2008

Flow and Heat Transfer in a Cross-Linked Silicon Microchannel Heat Sink

R. Muwanga* and I. Hassan†
Concordia University, Montreal, Quebec H3G 1M8, Canada

DOI: 10.2514/1.33952

This paper presents the flow and heat transfer characteristics in a cross-linked silicon microchannel heat sink. The heat sink is composed of 45 channels, 269 μm wide × 283 μm tall, in a silicon substrate formed via deep reactive ion etching. A detailed discussion of the pressure drop data reduction is described, including characterization of the channel cross sections and methods to account for inlet and exit loss coefficients. No significant difference is observed in the pressure drop measurements between the cross-linked and standard heat sinks flowing air and water. The use of unencapsulated liquid crystal thermography was successfully used to obtain local heat transfer data with FC-72 as the working fluid. The heat transfer results show inflections in the thermal profile due to the cross links.

Nomenclature

A_{heated}	=	heated area of channels, m^2, 3.5 cm^2
D_h	=	hydraulic diameter, m
f	=	friction factor
H	=	height, m
h	=	heat transfer coefficient, $W/(m^2 \cdot °C)$
INT01	=	cross-linked heat sink
K	=	minor pressure loss coefficients
K_∞	=	pressure loss coefficient due to flow development
k	=	thermal conductivity, $W/(m \cdot °C)$
L	=	length, m
N_{chn}	=	number of channels
Nu	=	Nusselt number, with respect to hydraulic diameter
P	=	pressure, kPa
Q_{vol}	=	volumetric flow rate, m^3/s
q''	=	heat flux, W/m^2
Re	=	Reynolds number, with respect to hydraulic diameter
STR01, STR02	=	straight standard heat sink
T	=	temperature, °C
V	=	velocity, m/s
W	=	width, m
W_{tot}	=	total width of channel frontal area, m
y	=	spanwise location, m
z	=	streamwise location, m
α	=	channel aspect ratio, W/H
Δ	=	change in parameter between outlet and inlet
δ_{Si}	=	silicon wafer thickness
η	=	fin efficiency
ξ	=	pressure changes due to entry or exit of parallel channel sections
ρ	=	density, kg/m^3
σ	=	ratio of flow area to frontal area

Subscripts

b	=	fluid bulk condition
c	=	contraction
chn	=	channel parameter
e	=	expansion
in	=	inlet condition
w, i	=	inner surface
j	=	index counter
measured	=	measured parameter
w, o	=	outer wall
out	=	outlet condition
Si	=	silicon
w	=	channel wall (fin width)

Introduction

ONE of the emerging cooling approaches that addresses the increasing miniaturization of electronics is the microelectromechanical system (MEMS) based heat sink, which consists of a set of microchannels etched in a silicon wafer. Tuckerman and Pease [1] pioneered this device in the early 1980s using a wet etched 50 μm wide and 300 μm deep silicon microchannel heat sink. Under single-phase conditions flowing deionized water, they were able to demonstrate heat dissipation up to 790 W on a 1 cm^2 chip. Numerous studies of flows in microchannel arrays have since followed, using a variety of fabrication techniques, both conventional and MEMS based. For conventional techniques, the predominant microchannel array machining techniques include sawing and milling. A summary of the major microfabrication techniques available has been presented by Kandlikar and Grande [2]. Among these, bulk micromachining through wet or dry etching has been the main technique used.

Recently, there have been a number of investigations considering radical modifications to the standard straight microchannel heat sink for pumped cooling loops. Among these, single-phase flow studies have considered pin fins [3,4], fractal networks [5–7], and cross-linked channels [8–10]. Xu et al. [8] used a concept of gaps at cross links along 10 triangular channels of 155 μm hydraulic diameter. The objective here was to increase the heat transfer by introduction of a constantly redeveloping thermal boundary layer. They compared this configuration with a standard straight channel configuration. Temperature profiles for the straight channel had a constant rise, whereas, for the transverse section, they would rise, then drop at the cross connections giving a lower mean temperature. Additionally, the cross-linked design showed a lower pressure drop than the straight channel. Cho et al. [9] also studied a similar cross-linked configuration, however, with rectangular channels. Heat transfer

Received 8 August 2007; accepted for publication 28 December 2007.

*Test Research and Development Engineer, Department of Mechanical and Industrial Engineering; currently Intel Corporation, Chandler, Arizona. AIAA Member.

†Associate Professor, Department of Mechanical and Industrial Engineering; ibrahimH@alcor.concordia.ca.

studies considered localized heating to better simulate real chip conditions. Under single-phase flow, the cross-connected configuration showed better performance, but, contrary to the previous study, showed an increase in pressure drop. Colgan et al. [11] studied a configuration with fins rather than channels combined with multiple entries and exits along the flowpath. The fins were arranged in an in-line or staggered configuration and had sharp or blunt ends. The sharp vs blunt end configurations did not show any significant benefit, however, the staggered fins had a better thermal performance though a higher pressure drop.

A number of studies have been conducted in recent years to understand and improve the heat transfer performance of microchannel-based devices, and recent summaries may be found in [12–14]. There are discrepancies reported between microchannel results and the accepted correlations and trends for their macro counterparts. In addition, significant variations between the results of different investigators have been reported for the heat transfer coefficients and friction factor with no clear relationship in the differences in some instances [13]. Overall, a review of the literature indicates the need for additional and improved studies of heat transfer in mini- and microchannels [14].

The preceding review shows that work on novel micro-heat-sink configurations is only in its infancy and much work remains to improve on the various proposed concepts. As well due to the differences between microchannel and conventional channel results noted among researchers, the verification of the measurement approach is imperative for sound experimental work. The following presents the fabrication technique and measurement methodology of a cross-linked microchannel heat sink. It is similar to a standard microchannel heat sink with parallel channels, except that gaps are introduced at three locations along the channels. The purpose of the gaps is to allow fluid communication between channels at additional points other than entry or exit of the channel to minimize flow maldistribution under single- and two-phase flow conditions. The heat sink fluidic performance is benchmarked against a standard parallel microchannel heat sink.

Test Module Fabrication and Packaging

Heat Sink Fabrication

The heat sink dimensions were sized based on a thermal load of 25 W/cm^2, given a 3.5 cm^2 footprint area with a maximum temperature of 85°C. This is loosely based on the criterion laid out by Paris et al. [15] for the requirements of future micro/nanospacecrafts. The footprint area is taken as the plan area encompassing the channels (16×21.875 mm). Further constraints are that single-phase water is the working fluid and the maximum pressure available is 34.5 kPa (5 psi). The fabricated heat sinks consist of a silicon wafer with an SiO_2 layer for insulation. A glass cover of thickness 500 μm seals the chamber and is bonded to the silicon base piece containing the channels. The cover has eight 1-mm-diam holes for flow inlet and outlet, and will also allow for future work in flow visualization. A serpentine platinum heating element, 1 mm wide and 186 mm long is deposited on the backside of the channel base to simulate the heated chip. A schematic of these components is shown in Fig. 1. An outline of the fabrication steps is presented in Fig. 2.

Heat Sink Packaging for Measurement

Three heat sinks were used in the present investigations: two standard heat sinks (STR01 and STR02) and a cross-linked heat sink (INT01). The fabricated channel dimensions were optically verified before packaging onto the support. A comparison of the design and measured dimensions is shown in Table 1.

The heating element has been designed for a nominal resistance of 90 Ω, with a potential applied serially through the entire length of the serpentine. However, the actual resistance was found to be approximately 16 times greater. To account for this, the potential is applied in parallel through the 11 strips of the serpentine. Two different heat sink supports were used. The first support is shown in Fig. 3a with the inlet and outlet chambers, and the pressure and

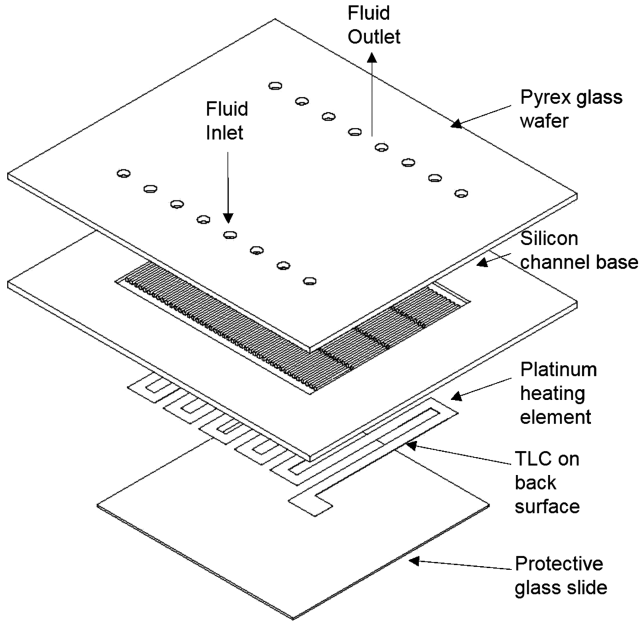

Fig. 1 Microchannel heat sink package components.

temperature taps. It is fabricated from Teflon due to its high temperature limits, as well as its low thermal conductivity and high electrical resistance. The chips were originally intended to be directly mounted to the Teflon base piece with gaskets for sealing. However, during sealing attempts, chips easily broke if misaligned when applying the required compressive loading for the gaskets. Rather

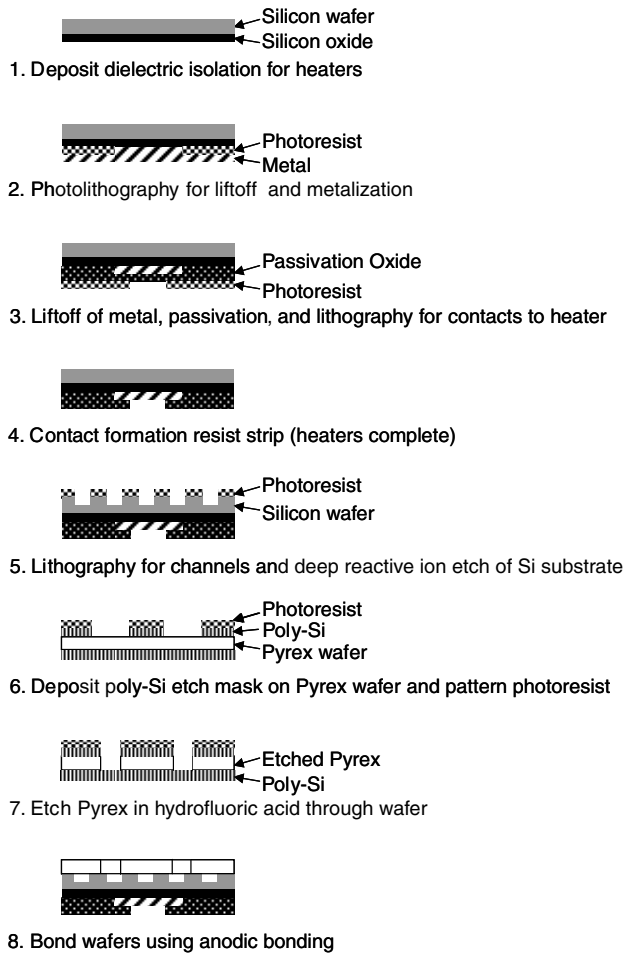

Fig. 2 Microchannel heat sink fabrication.

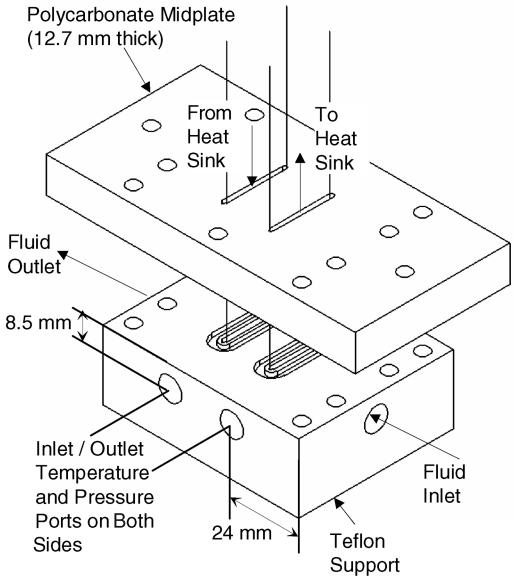

a) Teflon base and polycarbonate midplate; dimensions in millimeters

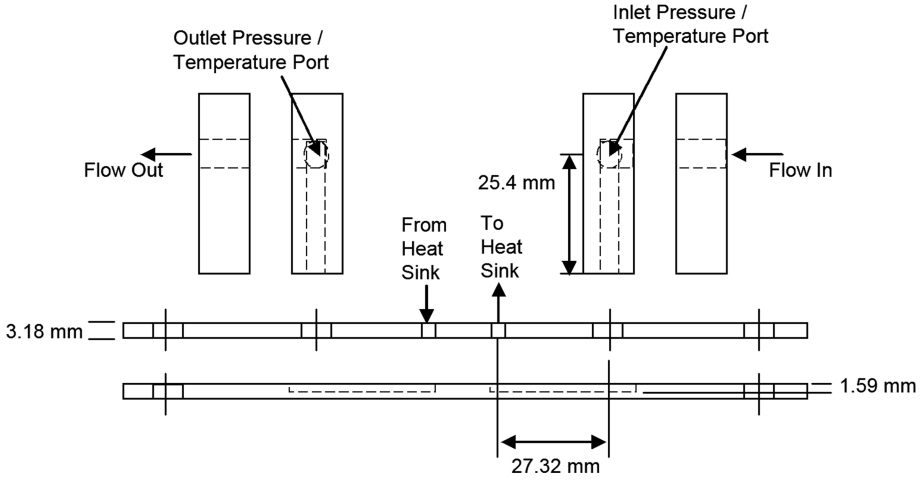

b) Polycarbonate support

Fig. 3 Microchannel heat sink support modules.

then, a rigid midplate with two slots for fluid transfer was introduced for the chips to be permanently bonded onto, before transferring to the Teflon base. This midplate, which is easily handled, is sealed to the Teflon base using a silicone-based adhesive with a high temperature limit or the gaskets. The midplate is transparent to verify that the sealant between the chips and the midplate does not leak into the heat sink portholes, and polycarbonate is selected due to its higher temperature limits. The second support, shown in Fig. 3b, was designed to allow for flow visualization and microparticle imaging velocimetry experiments. All parts are manufactured from transparent polycarbonate to provide sufficient temperature limits with optical access. A top plate 3.18 mm (1/8″ sheet) thick supports the heat sink. A second base plate, also 3.18 mm thick, has a 1.59 mm deep slot machined to allow fluid transport from the pressure/temperature measurement ports to and from the heat sink. Thin plates were used to accommodate the working distance of the microscope objectives. The plates were bonded together using a polycarbonate cement (SC-325 Cadillac Plastic and Chemical Company). The heat sink was bonded to the top plate using a transparent UV adhesive recommended for elevated temperatures with moisture content.

Two 1.5-mm-diam Type-T (Omega special error limits material) thermocouples are placed in each plenum chamber to measure the bulk fluid temperature. An Omega model PX821 pressure transducer with a rating of 0–34.5 kPa (0–5 psi) tracks the differential pressure across the test section.

Test Facility

A schematic of the main components used in the closed loop test facility is shown in Fig. 4. Distilled water, FC-72, and air are used as the working fluids. Different fluids were used depending on their compatibility with the sealing mechanism. For the liquid line, water or FC-72 enters the loop from the degassing tank and is continuously circulated by a magnetically coupled gear pump. For the present experiments, the degassing tank was only used to store the fluid, with no degassing procedure applied. The pump is equipped with a variable speed drive allowing for a flow range up to 300 ml/min, with a maximum pressure of 517 kPa (75 psi). A nutating digital output flowmeter provided by DEA Engineering is used to monitor the flow rate. This meter outputs a 5 V square wave signal at a frequency proportional to the time for the nutator to complete one cycle. The flowmeter has been calibrated using the weighing method, and has a reliable range from 10 to 250 ml/min. Upstream of the flowmeter is a 15 μm filter which is used to remove any accumulating particles. In addition, a preheater is located at the inlet of the test section for additional flow temperature control. At the exit of the test section, a water-cooled heat exchanger is used to restore the temperature of the fluid. For the air line, the air enters from the buildings source with a pressure of approximately 552 kPa (80 psi) after being filtered and dried. A regulator reduces the pressure to the range applicable for the experiments (34–69 kPa). The flow rate is adjusted by a needle valve and a mass flowmeter (Omega model

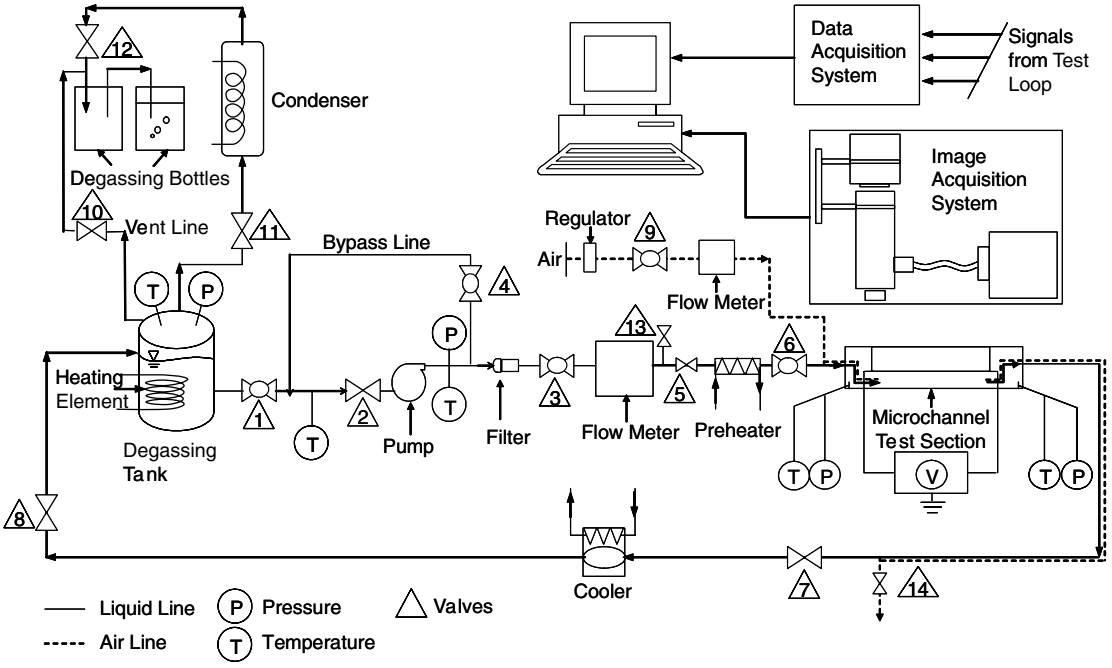

Fig. 4 Test facility.

FMA-1609) tracks the air flow rate. The air exits to the atmosphere just after exiting the test module.

The output from the various sensors is monitored through an automated data acquisition system using LabVIEW software. The data acquisition hardware consists of National Instrument's SCXI 1000 signal conditioning unit, with the appropriate modules, as well as the NI 6052E 16-bit 333 kHz data acquisition card. Heater power is provided by two BK Precision dc power supplies (Model 1623A) operating in parallel mode, and each with a voltage range of 0–60 V and a maximum current rating of 1.5 A.

A detailed view of the image acquisition apparatus is shown in Fig. 5. Light originating from the illuminator box is directed through a single fiber optic cable. This has the advantage of keeping any heat generated by the light source away from the thermochromic liquid crystal (TLC) coated surface. An EKE configured lamp is used with a color temperature rating of 3250 K. Light passes through a polarizer just before entering the zoom lens casing. Within the casing, it is deflected to the test surface by a beam splitter. Depending on the magnification required, the light may pass through an infinity corrected objective for high-resolution measurements or else through the default auxiliary lens. Upon reflection from the surface, the light is circularly polarized. It passes into the zoom lens through the analyzer and is directed to the charge-coupled device (CCD) camera. The crossed polarizing lens pair is available to obtain improved image quality. The light reflected by the TLC material is circularly polarized and thus travels through the crossed polarizing pair essentially unaffected. The acquired image is then transferred directly to the computer as a National Television System Committee (NTSC) signal through a single bayonet Neill–Concelman (BNC) cable. An liquid crystal display (LCD) television is used for real-time

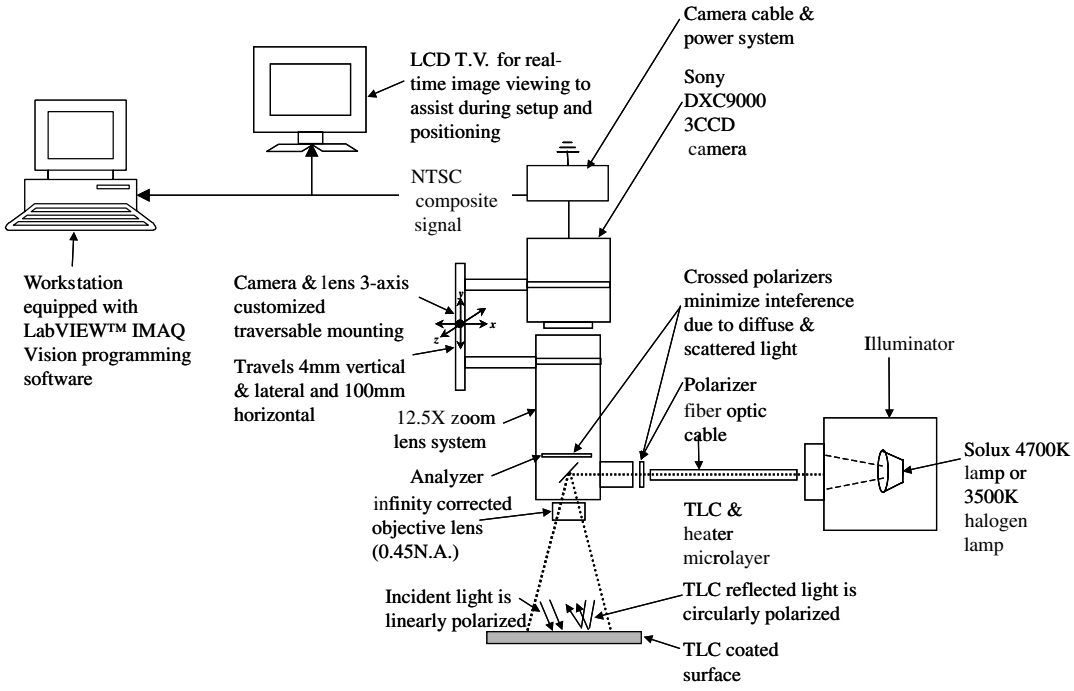

Fig. 5 Schematic of the image acquisition system.

monitoring and for positioning. The video signal used in the television loop comes from a separate output line in the camera, and the benefit of this is to minimize the accumulated noise that can occur by transferring the desired video signal through many components. Image acquisition is obtained using a Sony 3-CCD analog camera. The camera is connected to a variable zoom microscopic video lens. The camera lens combination is mounted onto a 3-axis traverse through variable length stages each with approximately a 1 μm resolution, which allows for fine tuning of the position and focusing.

Methodology

Single-Phase Pressure Drop

The pressure taps are located at some distance from the channel inlets and exits, and so contain additional pressure loss components due to the inlet and outlet chamber circuitry. These are accounted for through loss factors K_i for area changes and bends, and are obtained from Munson et al. [16]. Additional losses will be incurred due to the channel entry and exit and flow acceleration. These are estimated using the methodology outlined by Kays and London [17] for flows in compact heat exchangers. Finally, as the flow at entry is not fully developed, this is also considered. In summary, the pressure drop in the channels ΔP_{chn} is obtained as follows:

$$\Delta P_{\text{measured}} = \Delta P_{\text{chn}} + \left[\xi_{\text{in}} + 2\left(\frac{\rho_{\text{in}}}{\rho_{\text{out}}} - 1\right) - \frac{\rho_{\text{in}}}{\rho_{\text{out}}}\xi_{\text{out}} + K_{\infty}\right]\frac{(\rho V^2)_{\text{chn,in}}}{2} + \text{minor losses} \tag{1}$$

where

$$\xi_{\text{in}} = K_c + 1 - \sigma^2 \tag{2}$$

$$\xi_{\text{out}} = 1 - \sigma^2 - K_e \tag{3}$$

and

$$\sigma = \frac{N_{\text{chn}} W_{\text{chn}} H_{\text{chn}}}{W_{\text{total}} H_{\text{chn}}} \tag{4}$$

and where

$$\text{minor losses} = \sum_j K_j \frac{(\rho V^2)_j}{2} \tag{5}$$

The loss factors used in the preceding equations are from experiments in macrosize configurations. These may not be fully appropriate for all the present conditions, particularly for the channel inlet and exit losses. Nevertheless, they are used, as there are currently no correlations for microconfigurations readily available.

For comparison with theoretical predictions, the pressure drop across the channels may be obtained from

$$\Delta P_{\text{chn}} = 4f\frac{L}{D_h}\frac{\rho_{\text{in}}}{\rho_{\text{mean}}}\frac{(\rho V^2)_{\text{chn,in}}}{2} \tag{6}$$

The friction factor is obtained from Shah and London [18] and, for a rectangular duct of 0.95 aspect ratio, is calculated to be approximately 14.25. For accurate prediction of the pressure drop, accurate determination of the channel dimensions is required, particularly the cross section. This may be done through nondestructive and destructive optical measurement, and both are used in the present investigations. In the first case, the width is obtained from a top view image and the depth is obtained from focusing on the top and bottom surfaces. This approach can be expected to provide good measurement of the width, however, the depth measurement will be slightly subjective. The alternative approach is obtaining the dimensions from cross sections of the heat sink. This approach, however, is destructive and therefore not favorable. The results showed both procedures, however, to be in good agreement with each other.

Inspection of the channel cross sections showed that they are not purely rectangular as assumed in the prediction calculations. At the inlet and exits, the channels have a slight flare, as shown in the heat sink top view of Fig. 6a. Because of this flare, the cross sections at the inlet and exits are trapezoidal with taper angles as low as 85 deg. This characteristic is depicted in Fig. 6b. In the channel core, however, the channels are found to not have a strongly tapered angle, but do have curved edges. Figure 6c shows a cross section of the core and shows the locations used for approximating the dimensions. These deviations in fabrication have been noted by some other researchers, such as Steinke and Kandlikar [19], and the present inspection shows the importance of determining the "as fabricated" channel dimensions. In addition, it is preferable to perform such measurements before sealing the heat sink, so that destructive testing does not have to be performed, unless the sealing process has an influence on the final dimensions.

Single-Phase Heat Transfer

To evaluate the heat transfer performance, a recently developed liquid crystal thermography system is used. Thermochromic liquid crystal thermometry is a nonintrusive technique based on the changing pitch size of the helical molecular structure of the material during temperature change. When illuminated with white light, TLCs will reflect light of wavelength proportional to the temperature they are experiencing, and this reflected wavelength is proportional to the instantaneous pitch between molecular layers. Additional information about the characteristics of liquid crystals and their use in thermometry and heat transfer may be found in [20,21].

The unencapsulated liquid crystal material used is provided by LCR–Hallcrest. The TLC material nominally has a red start of 40°C with a bandwidth of 10°C. The TLC material is applied onto the back

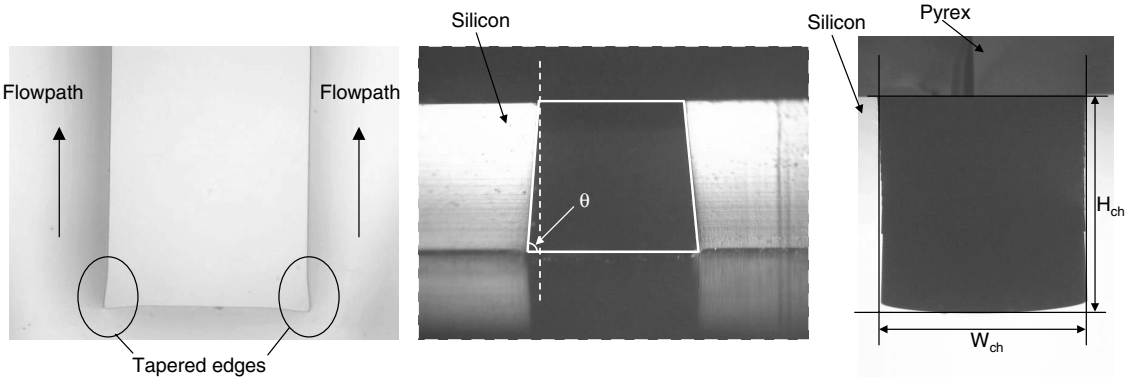

Fig. 6 Channel inspection a) tapered edges, b) trapezoidal cross section at entry/exit, c) cross section in core.

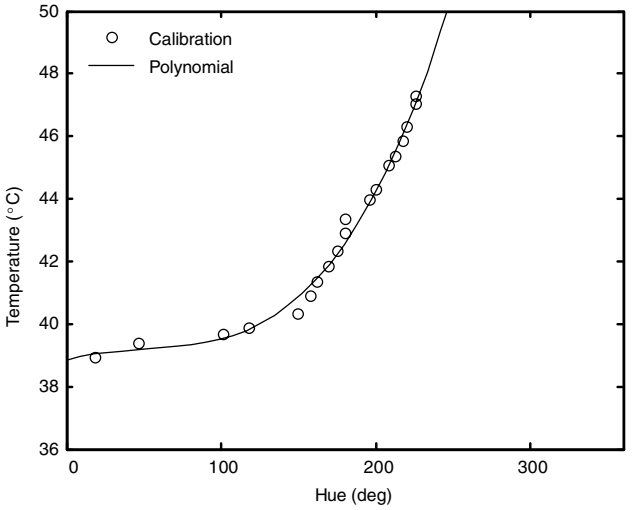

Fig. 7 Calibration curve.

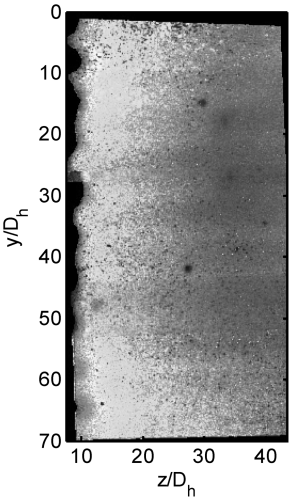

Fig. 8 Preprocessed heat sink TLC thermal map, consists of four images joined and binary filtered, Reynolds number ∼41, $Q \sim 11.5$ W/cm^2.

surface of the silicon using a Badger Model 100 independent action airbrush, and with the material dissolved in acetone with concentrations by weight of 20:1 (solvent to TLC). A black paint coating is applied before the TLC coating for improved color vibrancy. To obtain quantitative thermal data from the TLC response, a calibration of the material is required, which involves quantitatively relating the observed color to the material temperature. Different methods are available for quantifying the color observed and in the current work, the hue angle is taken as the color descriptor. The hue to temperature conversion is similar to that outlined by Muwanga and Hassan [22]. Calibration is performed by circulating heated liquid flow at 60 ml/ min through the heat sink. Temperature differences between the inlet and outlet were low at less than 0.4°C. Figure 7 shows a sample calibration curve, showing the good fit of the derived polynomial. For pixels with hue values greater than 300 deg, the negative hue angle is used to account for scatter at these values. Image capture covers a region of 9.94×7.45 mm, yielding a resolution of 10 μm/pixel. To map the entire heat sink, three locations are traversed in the spanwise direction. To enable automated image preprocessing and presentation, regions of the image that were not active had their pixel values set to zero. This is done by applying a binary filter with the regions marked up manually. On completion, the images from a single case at all four locations are joined in an automated procedure. Where there is overlap, the average pixel value is used. Figure 8 shows a sample of a preprocessed TLC image map of the heated surface.

Evaluation of the local heat transfer coefficient is through assuming the heat sink will behave as a one-dimensional fin with insulated ends. Such an approach has been presented by Qu and Mudawar [23], and a similar approach is used as follows:

$$q'' W_{\text{cell}} L_{\text{plan}} = h(T_{w,i} - T_b)(W_{\text{chn}} + 2\eta H_{\text{chn}})(4L_{\text{chn}}) \tag{7}$$

$$\eta = \frac{\tanh(mH_{\text{chn}})}{mH_{\text{chn}}} \tag{8}$$

$$m = \sqrt{\frac{h}{k_{\text{Si}} W_w/2}} \tag{9}$$

$$W_{\text{cell}} = W_{\text{chn}} + 2(W_w/2) \tag{10}$$

A unit cell $W_{\text{cell}}/2$ consists of a single channel with half the wall thickness on either side ($W_w/2$). The aforementioned neglects the heat transfer contribution within the cross-link paths and is used out of convenience, as the exact location of the cross links is not easily determined from the back surface of the chips. The heat transfer coefficient is evaluated iteratively to an accuracy of $1e^{-3}$. The inner wall temperature is obtained from a one-dimensional heat transfer approximation as follows:

$$T_{w,i} = T_{w,o} - \frac{q''(\delta_{\text{Si}} - H_{\text{chn}})}{k_{\text{Si}}} \tag{11}$$

Under single-phase flow conditions, the power to the fluid is obtained based on its enthalpy rise. Subsequently, the heat flux on the outer surface is then obtained as

$$q'' = \frac{Q_{\text{vol}}(\rho_{\text{out}} C p_{\text{out}} T_{\text{out}} - \rho_{\text{in}} C p_{\text{in}} T_{\text{in}})}{A_{\text{heated}}} \tag{12}$$

Uncertainty

Uncertainties for derived parameters have been calculated using similar methods to those described by Kline and McClintock [24]. The uncertainty in the TLC temperature is calculated using similar methods discussed in Muwanga and Hassan [22]. TLC temperature measurement uncertainties are estimated to range from ±1.1 to ±1.5°C. Typical uncertainties in the Nusselt number are estimated at 9%. Uncertainties in pressure drop measurement are ±0.03 kPa, based on instrument specifications, ±0.7°C for fluid temperature measurement based on manufacturer specifications of the combined measurement system, and ±2.25 ml/ min for the flow rate.

Results

Pressure Drop

Pressure drop measurements are carried out with both air and water in a flow range of 1–5 standard liters per minute and 10–200 ml/ min, respectively. These measurements were carried out with the support system in Fig. 3a. Initial liquid pressure drop results showed a significant deviation from theoretical predictions at low Reynolds numbers. Comparison with the air data suggested that the deviations are not likely due to channel dimensions or sensors. A physical difference between the water and air is the existence of surface tension in the case of water. Some recent works have shown that the congestion of a bubble in microchannels can pose a significant increase on the pressure drop [25]. If this is indeed the case, methods to alleviate it include applying a high liquid pressure, vibration of the channels, or a deaerating technique such as heating the flow. The chosen approach was to run at high flow rate to increase the pressure, with the fluid at an elevated temperature. Through this method, it was confirmed that the majority of the deviation from theoretical predictions was due to bubble congestion in the channels. These bubbles arose during filling of the test channels with liquid. Visualization would have also verified this, however, in cases such as

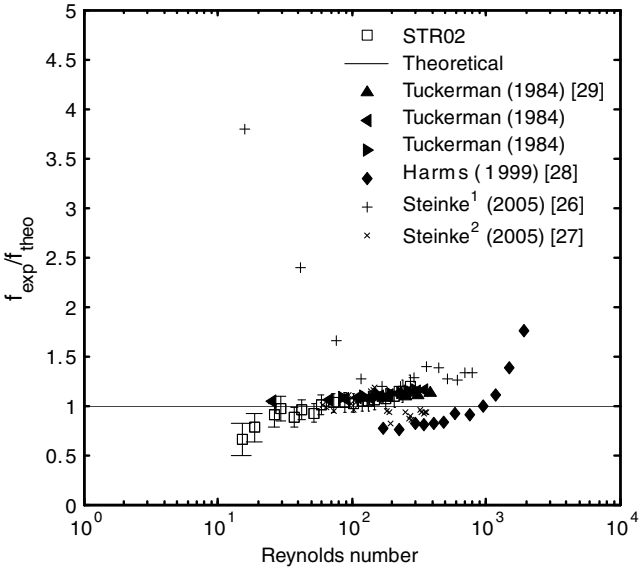

Fig. 9 Ratio of experimental to theoretical friction factor vs Reynolds number, comparison with other researchers flowing water in parallel silicon microchannels.

the present case where this was not possible, the aforementioned procedure proved to be a valuable approach.

Figure 9 compares the difference between measured and predicted friction factors from a number of microchannel studies [26–29]. All studies used parallel silicon channels flowing water and accounted for entrance and exit losses in a manner similar to what has been presented. The present measurements are found to be within the range of those obtained by other researchers. At higher Reynolds number, there is a consistent trend of an increasing deviation from predictions. This is likely due to the loss factors not being fully appropriate for parallel microchannel configurations. Future works should look into obtaining loss factors appropriate for micro-geometries. Figures 10a and 10b compare the pressure drop characteristics between the standard and cross-linked heat sink. The difference in pressure drop is observed to be negligible over the flow range investigated and no discernible benefit or detriment of the cross-linked scheme is observed.

Heat Transfer

Heat transfer measurements were carried out with FC-72 at Reynolds numbers ranging from 142 to 559 using the support system

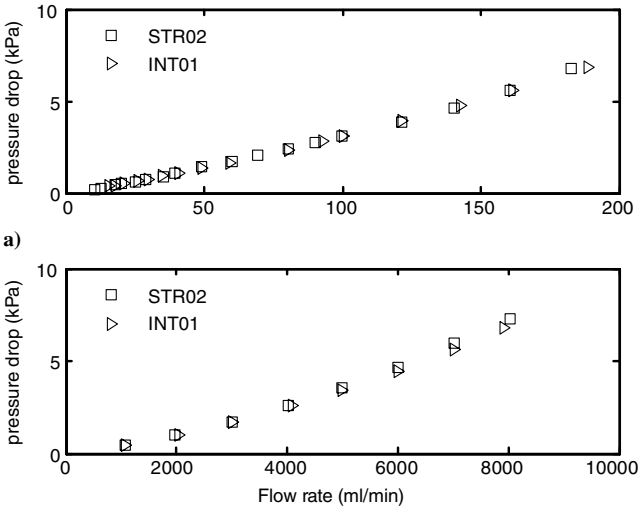

Fig. 10 Pressure drop vs flow rate for standard vs cross-linked microchannel heat sinks flowing water and air.

of Fig. 3b. Successful measurements were obtained only with the cross-linked heat sink, due to leakage and fracture of the standard heat sinks. Local wall temperatures and Nusselt values are presented in Figs. 11–14. Also presented in the figures are the calculated local fluid bulk temperatures and the approximate location of the cross links. The results are spanwise averages centered at 17.6, 35.3, and 52.9 y/D_h and averaged over 250 pixels, which correspond to one-fifth of the height. Negligible differences are observed in the wall temperatures and Nusselt values between the different spanwise locations considered. For the Reynolds range covered, the wall temperature rises nonlinearly and peaks just after the second cross link. In all cases, a slight drop in wall temperature is observed at the third cross link. Finally, a slight change in slope is observed at the first cross link. Overall, the cross-link influence on heat transfer for the present configuration and Reynolds number range is observed, however, it is minimal. Xu et al. [8] observed a dramatic change in their averaged streamwise wall temperature and Nusselt values from their experiments with cross-linked triangular channels. This was attributed to a redeveloping thermal boundary layer. Their cross-link widths, however, were approximately three times wider than the channel width, and their configuration included five cross-link paths. Similarly, thermal boundary-layer redevelopment is the likely cause of the observed inflections in temperature and Nusselt number profiles. However, given the narrower cross-link widths in the

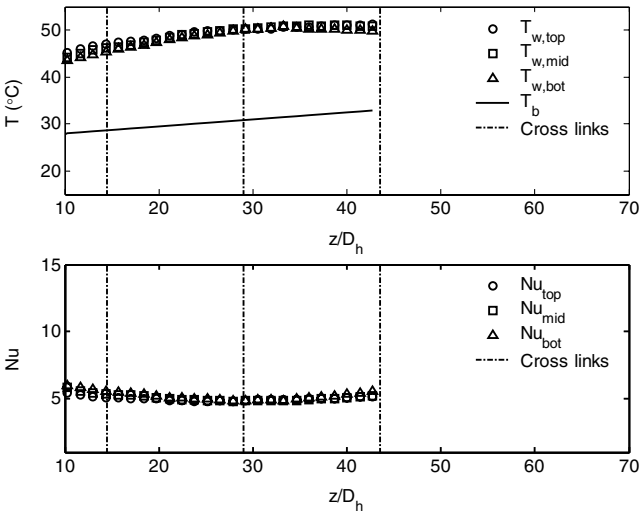

Fig. 11 Local wall temperatures and Nusselt numbers at various spanwise locations, $Re = 142$, INT01 flowing FC-72.

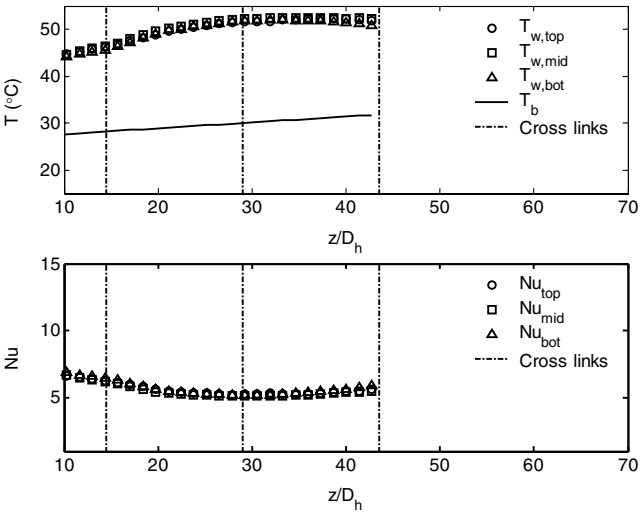

Fig. 12 Local wall temperatures and Nusselt numbers at various spanwise locations, $Re = 210$, INT01 flowing FC-72.

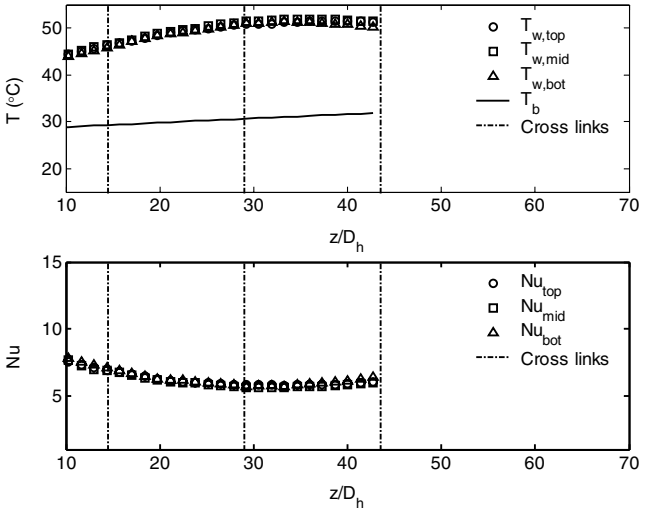

Fig. 13 Local wall temperatures and Nusselt numbers at various spanwise locations, $Re = 307$, INT01 flowing FC-72.

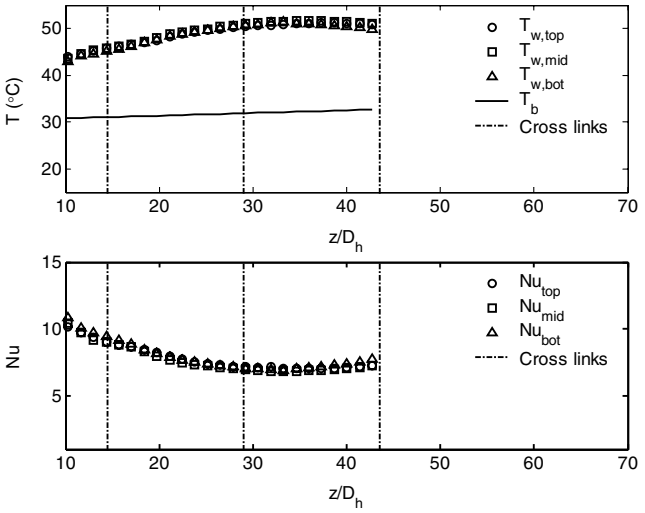

Fig. 14 Local wall temperatures and Nusselt numbers at various spanwise locations, $Re = 559$, INT01 flowing FC-72.

present work (cross-link width $\approx$ channel width), minimal influences are observed.

Figure 15 compares the averaged streamwise Nusselt number based on the central region ($35.3\ y/D_h$) with the theoretical solution for four-wall heated channels given by Shah and London [18]. This solution assumes hydrodynamically fully developed flow. From this figure, it is observed that the results correlate similarly with the nondimensional parameters of laminar thermally developing flows.

Conclusions

This paper has presented the single-phase flow characteristics comparing a cross-linked microchannel heat sink with a standard heat sink. Relatively good agreement was obtained between air and water adiabatic pressure measurements compared with theoretical predictions after accounting for inlet and outlet losses. No significant flow differences were observed between a standard and a cross-linked heat sink scheme for the cross-linked spacing investigated (cross-link width $\approx$ channel width).

Heat transfer measurements under single-phase conditions were successfully obtained using a recently developed liquid crystal thermography method. Variations in the streamwise thermal profiles were observed due to the cross-links. These variations, however, were minor due to the narrow width of the cross links used. Future work will investigate the single- and two-phase heat transfer of the cross-linked scheme under a wide range of conditions and with varying gap widths.

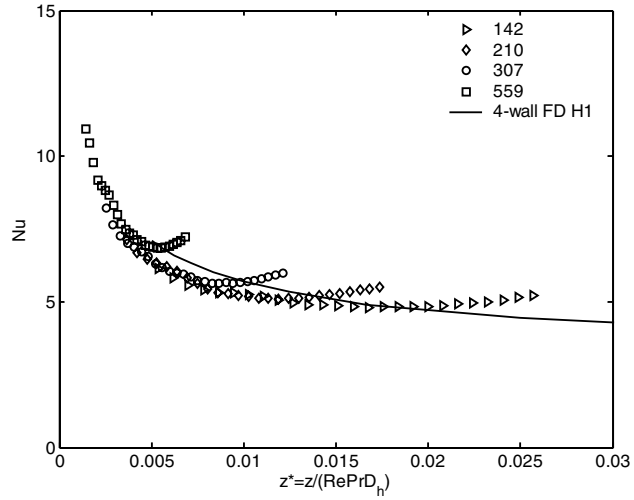

Fig. 15 Local Nusselt numbers vs nondimensional streamwise distance at various Reynolds numbers, INT01 flowing FC-72.

References

[1] Tuckerman, D. B., and Pease, R. F. W., "High-Performance Heat Sinking for VLSI," *Electron Device Letters*, Vol. 2, No 5, 1981, pp. 126–129.

[2] Kandlikar, S. G., and Grande, W. J., "Evolution of Microchannel Flow Passages: Thermohydraulic Performance and Fabrication Technology," *Heat Transfer Engineering*, Vol. 24, No 1, 2003, pp. 3–17. doi:10.1080/01457630304040

[3] Kosar, A., and Peles, Y., "Thermal-Hydraulic Performance of MEMS-Based Pin Fin Heat Sink," *Journal of Heat Transfer*, Vol. 128, No. 2, 2006, pp. 121–131. doi:10.1115/1.2137760

[4] Peles, Y., Kosar, A., Mishra, C., Kuo, C., and Schneider, B., "Forced Convective Heat Transfer Across a Pin Fin Micro Heat Sink," *International Journal of Heat and Mass Transfer*, Vol. 48, No. 17, 2005, pp. 3615–3627. doi:10.1016/j.ijheatmasstransfer.2005.03.017

[5] Chen, Y., and Cheng, P., "Experimental Investigation on the Thermal Efficiency of Fractal Tree-Like Microchannel Nets," *International Communications in Heat and Mass Transfer*, Vol. 32, No. 7, 2005, pp. 931–938. doi:10.1016/j.icheatmasstransfer.2005.02.001

[6] Alharbi, A., Pence, D., and Cullion, R., "Thermal Characteristics of Microscale Fractal-Like Branching Channels," *Journal of Heat Transfer*, Vol. 126, No 5, 2004, pp. 744–752. doi:10.1115/1.1795236

[7] Pence, D. V., "Reduced Pumping Power and Wall Temperature in Microchannel Heat Sinks with Fractal-Like Branching Channel Networks," *Microscale Thermophysical Engineering*, Vol. 6, No. 4, 2002, pp. 319–330. doi:10.1080/10893950290098359

[8] Xu, J. L., Gan, Y. H., Zhang, D. C., and Li, X. H., "Microscale Heat Transfer Enhancement Using Thermal Boundary Layer Redeveloping Concept," *International Journal of Heat and Mass Transfer*, Vol. 48, No. 9, 2005 pp. 1662–1674. doi:10.1016/j.ijheatmasstransfer.2004.12.008

[9] Cho, E. S., Koo, J., Jiang, L., Prasher, R. S., Kim, M. S., Santiago, J. G., Kenny, T. W., and Goodson, K. E., "Experimental Study on Two-Phase Heat Transfer in Microchannel Heat Sinks with Hotspots," *Annual IEEE Semiconductor Thermal Measurement and Management Symposium*, Inst. of Electrical and Electronic Engineers, New York, 2003 pp. 242–246.

[10] Jiang, L., Koo, J. M., Wang, E., Bari, A., Cho, E. S., Ong, W., Prasher, R. S., Maveety, J., Kim, M. S., Kenny, T. W., Santiago, J. G., and Goodson, K. E., "Cross-Linked Microchannels for VLSI Hotspot Cooling," *Proceedings of the ASME International Mechanical Engineering Congress and Exposition*, American Society of Mechanical Engineers, Fairfield, NJ, 2002 pp. 13–17.

[11] Colgan, E. G., Furman, B., Gaynes, M., Graham, W., Labianca, N., Magerlein, J. H., Polastre, R. J., Rothwell, M. B., Bezama, R. J., Choudhary, R., Marston, K., Toy, H., Wakil, J., Zitz, J., and Schmidt, R., "Practical Implementation of Silicon Microchannel Coolers for High Power Chips," *Annual IEEE Semiconductor Thermal Measurement and Management Symposium, 21st Annual IEEE Semiconductor Thermal Measurement and Management Symposium*, Inst. of Electrical and Electronic Engineers, New York, 2005 pp. 1–7.

[12] Zohar, Y., "Microchannel Heat Sinks" *The MEMS Handbook*, edited by M. Gad-el-Hak, McGraw–Hill, New York, 1998 pp. 32-1–32-30.

[13] Mehendale, S. S., Jacobi, A. M., and Shah, R. K., "Fluid Flow and Heat Transfer a Micro- and Meso- Scales with Application to Heat Exchanger Design," *Applied Mechanics Reviews*, Vol. 53, No. 7, 2000, pp. 175–193.

[14] Sobhan, C. B., and Garimella, S. V., "Comparative Analysis of Studies on Heat Transfer and Fluid Flow in Microchannels," *Heat Transfer and Transport Phenomena in Microscale, Proceedings of the International Conference on Heat Transfer*, Begell House, Redding, CT, 2000, pp. 80–92.

[15] Paris, D. A., Birur, C. G., and Green A. A., "Development of MEMS Microchannel Heat Sinks for Micro/Nano Spacecraft Thermal Control," *Proceedings of the International Mechanical Engineering Congress and Exposition (IMECE)*, American Society of Mechanical Engineers, Paper 2002-342937, 2002.

[16] Munson, B. R., Young, D. F., and Okiishi, T. H., *Fundamentals of Fluid Mechanics*, 4th ed., Wiley, New York, 2002, pp. 480–489.

[17] Kays, W. M., and London, A. L., *Compact Heat Exchangers*, McGraw–Hill, New York, 1964, pp. 32–33.

[18] Shah, R. K., and London, A. L., "Laminar Flow Forced Convection in Ducts," *Advances in Heat Transfer*, Academic Press, New York, 1978.

[19] Steinke, M. E., and Kandlikar, S. G., "Single-Phase Liquid Heat Transfer in Microchannels," *3rd International Conference on Microchannels and Minichannels*, American Society of Mechanical Engineers, New York, June 2005, p. 12.

[20] Ireland, P. T., and Jones, T. V., "Liquid Crystal Measurements of Heat Transfer and Surface Shear Stress," *Measurement Science and Technology*, Vol. 11, No. 7, 2000, pp. 969–986. doi:10.1088/0957-0233/11/7/313

[21] Hallcrest Product Information, DS-001–DS-010, LCR/Hallcrest, Glenview, IL, 2000, http://www.hallcrest.com/randt.cfm.

[22] Muwanga R., and Hassan, I., "Local Heat Transfer Measurements in Microchannels Using Liquid Crystal Thermography: Methodology Development and Validation," *Journal of Heat Transfer*, Vol. 128, No. 7, 2006, pp. 617–626. doi:10.1115/1.2193541

[23] Qu, W., and Mudawar, I., "Flow Boiling Heat Transfer in Two-Phase Micro-Channel Heat Sinks, 1: Experimental Investigation and Assessment of Correlation Methods," *International Journal of Heat and Mass Transfer*, Vol. 46, No. 15, 2003, pp. 2755–2771. doi:10.1016/S0017-9310(03)00041-3

[24] Kline, J., and McClintock., F. A., "Describing Uncertainties in Single-Sample Experiments," *Mechanical Engineering*, Vol. 75, No. 1, 1953, pp. 3–8.

[25] Kim, D. S., Lee, K., Kwon, T. H., and Lee, S. S., "Micro-Channel Filling Flow Considering Surface Tension Effect," *Journal of Micromechanics and Microengineering*, Vol. 12, No. 3, 2002, pp. 236–246. doi:10.1088/0960-1317/12/3/307

[26] Steinke, M. E., and Kandlikar, S. G., "Single-Phase Liquid Friction Factors in Microchannels," *3rd International Conference on Microchannels and Minichannels*, American Society of Mechanical Engineers, New York, June 2005, p. 10.

[27] Steinke, M. E., Kandlikar, S. G., Magerlein, J. H., Colgan, E., and Raisanen, A. D., "Development of an Experimental Facility for Investigating Single-Phase Liquid Flow in Microchannels," *3rd International Conference on Microchannels and Minichannels*, American Society of Mechanical Engineers, New York, June 2005, p. 10.

[28] Harms, T. M., Kazmierczak, M. J., and Gerner, F. M., "Developing Convective Heat Transfer in Deep Rectangular Microchannels," *International Journal of Heat and Fluid Flow*, Vol. 20, No. 2, 1999, pp. 149–157. doi:10.1016/S0142-727X(98)10055-3

[29] Tuckerman, D. B., Heat-Transfer Microstructures for Integrated Circuits," Ph.D. Dissertation, Stanford Univ., Dept. of Electrical Engineering, Stanford, CA, 1984.